

ATLAS Diboson Excesses Demystified in Effective Field Theory Approach

Doojin Kim ^a

Department of Physics, University of Florida, Gainesville, FL 32611, USA

Kyoungchul Kong ^b

*Department of Physics and Astronomy,
University of Kansas, Lawrence, KS 66045, USA*

Hyun Min Lee ^c

Department of Physics, Chung-Ang University, Seoul 156-756, Korea

Seong Chan Park ^d

*Department of Physics, Sungkyunkwan University, Suwon 440-746, Korea
Korea Institute for Advanced Study, Seoul 130-722, Korea*

Abstract

We study the collider implication of a neutral resonance which decays to several diboson final states such as W^+W^- , ZZ , and $Z\gamma$ via a minimal set of effective operators. We consider both CP-even and CP-odd bosonic states with spin 0, 1, or 2. The production cross sections for the bosonic resonance states are obtained with the effective operators involving gluons (and quarks), and the branching fractions are obtained with the operators responsible for the interactions with electroweak gauge bosons. We demonstrate that each scenario allows for a broad parameter space which could accommodate the recently-reported intriguing excesses in the ATLAS diboson final states, and discuss how the CP states and spin information of the resonance can be extracted at the LHC run II.

Keywords: LHC, diboson, resonance, effective operators

^a immworry@ufl.edu

^b kckong@ku.edu

^c hminlee@cau.ac.kr

^d s.park@skku.edu

I. INTRODUCTION

Recently, the ATLAS collaboration has reported some excesses in searches for diboson resonances in the highly boosted final states with W^+W^- , $W^\pm Z$ and ZZ at the 8 TeV LHC with 20.3 fb^{-1} [1]. They have adapted boosted techniques to tag hadronically decaying W and Z gauge bosons, which strongly suppress the QCD dijet backgrounds. All three excesses emerge at $\sim 2 \text{ TeV}$ in the invariant mass distribution formed by two W - or Z -tagged fat jets. In response to the tantalizing experimental observations, several papers have already appeared taking this phenomenon as a new physics signature [4–28].

A typical recipe for a new physics model to explain the above-mentioned excesses is the introduction of two new heavy states: a charged particle and a neutral particle. The former takes care of the $W^\pm Z$ channel while the latter does the other two channels. However, given the fact that a large fraction of events belong to all three channels, it may be a reasonable attempt to fit the data only with a single new heavy resonance. As a matter of fact, Allanach, Gripaios and Sutherland recently investigated the diboson resonances in this direction: they basically introduced a likelihood function for the true signal in the W^+W^- , $W^\pm Z$, and ZZ channels and found that the maximum likelihood has zero events in the $W^\pm Z$ channel [11]. If this observation were true, ATLAS data would indicate a single neutral bosonic resonating particle rather than two, which show up in all three channels due to detector effects and misidentification of W^\pm and Z bosons. In the single particle interpretation, coincidence of the resonances at 2 TeV in the three channels can be easily understood. Keeping this minimality and simplicity of the single particle interpretation, we further investigate the possible classification of neutral resonances by considering different spins ($s = 0, 1$, and 2) and CP states in an effective field theory approach including a minimal set of operators for each case.

Our philosophy is basically the bottom-up approach, invoking effective operators that may be responsible for the W^+W^- and ZZ signals. As no spin information is available, we extensively consider spin-0, spin-1, and spin-2 resonances. Symmetries of the relevant operators also induce potential signals in different final states, encouraging experimental collaborations to look into the related channels for consistency.

In the following three sections, we examine scalar, vector, and tensor resonances in turn, focusing on viable parameter scans in conjunction with production cross sections and partial

decay widths of the resonance at hand. In Section V, we briefly make comments on kinematic correlations among the final state particles to extract spin, CP states, and coupling information of the resonance of interest and the proposed interactions. Section VI is reserved for a summary.

II. SPIN-0 RESONANCES

In our new physics interpretation, the resonance particle decays into two bosons so that the resonance itself should be a bosonic state with an integer spin. In this section, we begin with considering a spin-0 resonance and study the effects of its CP states with corresponding effective operators.

A. CP-even spin-0 resonance

A CP-even scalar resonance (henceforth denoted as S) in diboson channel could be well-parameterized by the following interaction Lagrangian:

$$\mathcal{L}_s = -\frac{1}{\Lambda} S \left(s_1 F_{\mu\nu}^Y F^{Y\mu\nu} + s_2 F_{\mu\nu}^W F^{W\mu\nu} + s_3 G_{\mu\nu}^a G^{a\mu\nu} \right), \quad (1)$$

where $F_{\mu\nu}^Y$ and $F_{\mu\nu}^W$ denote the field strength tensors for usual $U(1)_Y$ and $SU(2)_W$ gauge bosons *before* the electroweak symmetry breaking while $G_{\mu\nu}^a$ denotes the $SU(3)_c$ gluon field strength tensor with the color index $a = 1, 2, \dots, 8$.¹ The strengths of the above couplings are parametrized by s_1 , s_2 , and s_3 , respectively. The diquark coupling to the singlet scalar is induced through the mixing with the Higgs in the standard model (SM) for CP-even case or a pseudo-scalar in an extended model for CP-odd case. Hence, they are all Yukawa-suppressed, and we do not take them into consideration here.

Without loss of generality, we take $s_3 = 1$ by redefining Λ . The other coefficients, s_1 and s_2 , for $U(1)_Y$ and $SU(2)_W$ gauge kinetic terms, are redefined as relative strengths to s_3 . From the interactions in Eq.(1), we obtain the partial decay widths of S into $\gamma\gamma$, $Z\gamma$, ZZ ,

¹ A scalar particle such as gravi-scalar or radion [29–31] potentially provides diboson resonance and may have other signatures [32–34]. However, we found that the width of 2 TeV radion is unacceptably big to account for the ATLAS anomaly.

W^+W^- , and gg as

$$\left\{ \begin{array}{ll} \Gamma_S(\gamma\gamma) = \frac{|s_{\gamma\gamma}|^2 m_S^3}{4\pi\Lambda^2}, & s_{\gamma\gamma} = s_1 \cos^2 \theta_W + s_2 \sin^2 \theta_W, \\ \Gamma_S(Z\gamma) = \frac{|s_{Z\gamma}|^2 m_S^3}{8\pi\Lambda^2} (1 - x_Z^S)^3, & s_{Z\gamma} = (s_2 - s_1) \sin 2\theta_W, \\ \Gamma_S(ZZ) = \frac{|s_{ZZ}|^2 m_S^3}{4\pi\Lambda^2} \sqrt{1 - 4x_Z^S} (1 - 4x_Z^S + 6(x_Z^S)^2), & s_{ZZ} = s_2 \cos^2 \theta_W + s_1 \sin^2 \theta_W, \\ \Gamma_S(W^+W^-) = \frac{|s_{WW}|^2 m_S^3}{8\pi\Lambda^2} \sqrt{1 - 4x_W^S} (1 - 4x_W^S + 6(x_W^S)^2), & s_{WW} = 2s_2 \\ \Gamma_S(gg) = \frac{2|s_{gg}|^2 m_S^3}{\pi\Lambda^2}, & s_{gg} = s_3, \end{array} \right.$$

where m_S and θ_W denote the mass of CP-even scalar S and the usual Weinberg angle. Here and henceforth, we define the mass squared ratio of a heavy SM boson i (Z , W , or h) to a resonance R as

$$x_i^R \equiv \frac{m_i^2}{m_R^2}. \quad (3)$$

Obviously, in this parametrization, S is produced via gluon fusion followed by the decays into the above final states. Of potential experimental constraints, the two following conditions should be settled to be in the right ‘‘ball park’’ with respect to the recent ATLAS data:

- the total decay width should be within $\sim 10\%$ of the mass of the resonance [1],
- the signal production cross section should be as sizable as order of several fb [11].

In general, the *single* production cross section of a narrow resonance is proportional to the total decay width of the decaying particle. Therefore, demanding a sizable production cross section with a (relatively) smaller total decay width is *not* a trivial task. We remark that as discussed in the literature, reported excesses in all three diboson final states (W^+W^- , $W^\pm Z$ and ZZ) are not independent of one another, and the data in one channel may be contaminated by the data in the other channels due to detector effects. In Ref. [11], authors performed a general analysis of new physics interpretations of the recent ATLAS diboson excesses by computing a likelihood function for the true signal in the W^+W^- , $W^\pm Z$, and ZZ channels. They found that the maximum likelihood has zero events in the $W^\pm Z$ channel, i.e., one could fit the data in all three channels with a *single* neutral resonance in the final state with W^+W^- and ZZ . The likelihood is sufficiently flat and the required cross section (for 95% C.L.) is in the following range [11]:

$$\mathcal{O}(4 - 8) \text{ fb} \lesssim \sigma \cdot BR(W^+W^-) + \sigma \cdot BR(ZZ) \lesssim \mathcal{O}(20 - 24) \text{ fb}, \quad (4)$$

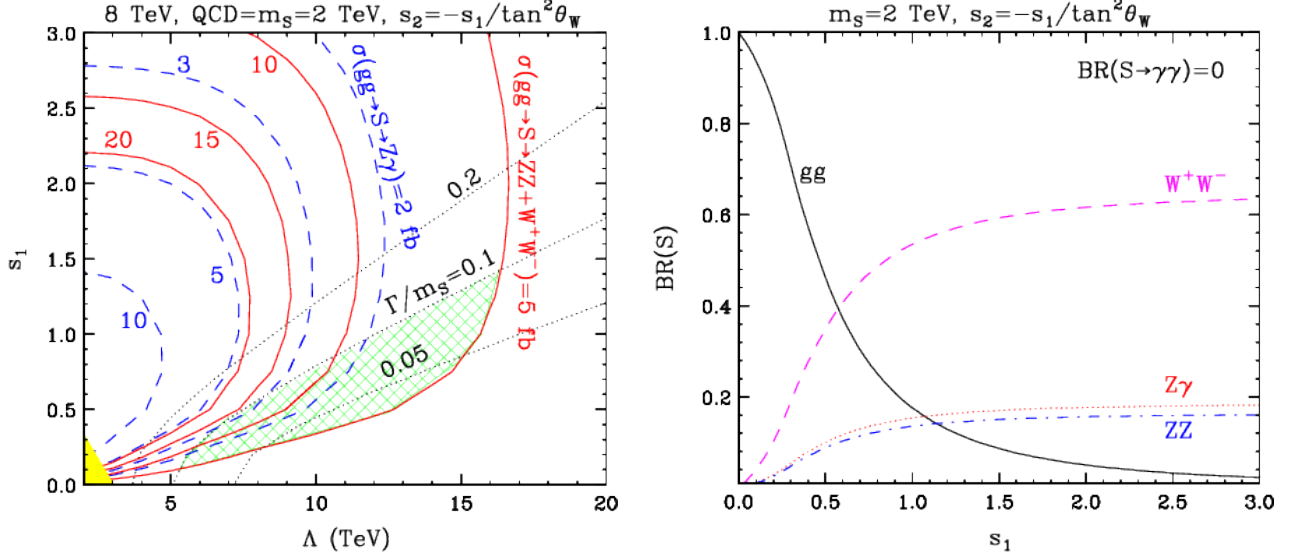


FIG. 1. The left panel shows production cross sections (in fb) of the CP-even scalar resonance in the final states with $W^+W^- + ZZ$ (red solid curves) and $Z\gamma$ (blue dashed curves). The black dotted curves represent the constraint of the total decay width, Γ/m_S . The dark yellow-shaded region is excluded by the dijet search and the light green-shaded region represents the allowed parameter space. The right panel shows branching fractions of the spin-0 resonance ($Z\gamma$, ZZ , W^+W^- , and gg by red dotted, blue dot-dashed, magenta dashed, and black solid curves, respectively) as a function of s_1 .

where σ is the single production cross section of the resonance. For our analysis with the case of the CP-even scalar, we first fix the mass of the scalar resonance, m_S , to 2 TeV, and then compute the signal cross section, $\sigma(pp \rightarrow S \rightarrow W^+W^- + ZZ)$, by varying three parameters, Λ , s_1 and s_2 ($s_3=1$). We find that in the majority of parameter space, the consistency (gauge invariance and Lorentz invariance) of the model predicts a large branching fraction into the diphoton final state. In particular, when two parameters have the same sign (i.e., $s_1 s_2 > 0$), diphoton rate ($\propto |s_{\gamma\gamma}|^2 = |s_1 \cos^2 \theta_W + s_2 \sin^2 \theta_W|^2$) turns out to be too large so that the model is severely constrained by current data at the 8 TeV LHC [35, 36].

Interestingly enough, the opposite case with $s_1 s_2 < 0$ constraint provides a way to reduce the diphoton rate as clear from Eq. (2). Especially, the condition of $s_1 \approx -\tan^2 \theta_W s_2$ gives $s_{\gamma\gamma} \approx 0$ thus vanishingly small diphoton final state, and the condition fixes the relative branching fractions as follows:

$$\begin{aligned}
& BR(W^+W^-) : BR(ZZ) : BR(Z\gamma) : BR(gg) \\
& \approx \frac{|s_1|^2}{4 \tan^4 \theta_W} : \frac{|s_1|^2 \cos^2 2\theta_W}{8 \sin^4 \theta_W} : \frac{|s_1|^2}{4 \tan^2 \theta_W} : 1.
\end{aligned} \tag{5}$$

We take this relation for illustration and calculate the relevant cross sections in the two dimensional parameter space of Λ vs. s_1 , although other relations can be straightforwardly analyzed. For the relevant data analysis (and remaining analyses throughout this paper), we employ Monte Carlo event generators `CalcHEP` [37] and `MadGraph5_aMC@NLO` [38]. In Fig. 1, we show production cross sections (in fb) of the CP-even scalar resonance in the final states with $W^+W^- + ZZ$ (red solid curves) and $Z\gamma$ (blue dashed curves). Contours of Γ/m_S are shown by black-dotted curves. The corresponding branching fractions are shown in the right panel as a function of s_1 . The dijet resonance searches provide constraints (at 95% C.L.) on the parameters, which are shown by the dark yellow-shaded region [39, 40]. Combining all constraints together, the allowed parameter space represented by the light green-shaded region might accommodate the diboson excesses. We remark that the exact relation of $s_1 = -\tan^2 \theta_W s_2$ is not required, and any minor deviation from this relation would be easily allowed as long as the associated diphoton rate is below the current limit [35, 36].

B. CP-odd spin-0 resonance

A pseudo-scalar or axion-like scalar (denoted as A) can couple to the SM gauge bosons through anomalies. The gauge interactions are parametrized in a way similar to the CP-even scalar case with one of the field strength tensors replaced by a dual field strength tensor:

$$\mathcal{L}_a = -\frac{1}{\Lambda} A \left(a_1 F_{\mu\nu}^Y \tilde{F}^{Y\mu\nu} + a_2 F_{\mu\nu}^W \tilde{F}^{W\mu\nu} + a_3 G_{\mu\nu} \tilde{G}^{\mu\nu} \right), \tag{6}$$

where the dual field strength tensors are defined as, for example, $\tilde{F}_{\mu\nu}^Y \equiv \frac{1}{2} \epsilon_{\mu\nu\rho\sigma} F^{Y\rho\sigma}$, and prefactors a_1 , a_2 , and a_3 denote the coupling constants which can be determined by anomalies for a global symmetry. For instance, $a_i/\Lambda = c_i \alpha_i / (8\pi f_A)$ ($i = 1, 2, 3$) with f_A being the breaking scale of a global $U(1)$ and $c_i = \sum_\alpha q_\alpha \ell_{G_i}(r_\alpha)$ where q_α is the global $U(1)$ charge of a heavy fermion and $\ell_{G_i}(r_\alpha)$ is the Dynkin index for a representation r_α under the SM gauge group G_i [41, 42].

The total decay width of the pseudo-scalar resonance [41] is given by the sum of partial decay widths into $\gamma\gamma$, $Z\gamma$, ZZ , W^+W^- , and gg :

$$\left\{ \begin{array}{ll} \Gamma_A(\gamma\gamma) = \frac{m_A^3}{4\pi\Lambda^2} |c_{\gamma\gamma}|^2, & c_{\gamma\gamma} = a_1 \cos^2 \theta_W + a_2 \sin^2 \theta_W, \\ \Gamma_A(Z\gamma) = \frac{m_A^3}{8\pi\Lambda^2} |c_{Z\gamma}|^2 (1 - x_Z^A)^3, & c_{Z\gamma} = (a_2 - a_1) \sin(2\theta_W), \\ \Gamma_A(ZZ) = \frac{m_A^3}{4\pi\Lambda^2} |c_{ZZ}|^2 (1 - 4x_Z^A)^{3/2}, & c_{ZZ} = a_2 \cos^2 \theta_W + a_1 \sin^2 \theta_W, \\ \Gamma_A(W^+W^-) = \frac{m_A^3}{8\pi\Lambda^2} |c_{WW}|^2 (1 - 4x_W^A)^{3/2}, & c_{WW} = 2a_2, \\ \Gamma_A(gg) = \frac{2m_A^3}{\pi\Lambda^2} |c_{gg}|^2, & c_{gg} = a_3, \end{array} \right. \quad (7)$$

where x_i^A is defined in Eq. (3). The case with the CP-odd scalar has similarities compared to the case with the CP-even scalar in the sense that the corresponding branching fractions are similar along with associated coefficients, and also we require $a_1 a_2 < 0$ to suppress the diphoton rate. Like the CP-even scalar case we simply choose $a_2 = -a_1 / \tan^2 \theta_W$, and demonstrate the resulting parameter scans in Fig. 2. We observe that all contours are similar to those in Fig. 1, except for the scale of Λ due to a larger cross section for the CP-odd scalar.

A couple of comments should be made here. Speaking of the unitarity bound for scalar resonances first, we observe that in both CP-even and CP-odd cases, the spin-0 resonance couples only to transverse modes of SM gauge bosons. Then, the unitarity cutoff can be just read from the coefficients of the effective operators, namely, of order $\max(\Lambda/s_i)$ and $\max(\Lambda/a_i)$ in CP-even and -odd cases, respectively, by power counting. Thus, as shown in Fig. 1 and Fig. 2, the unitarity cutoff is $\gtrsim \Lambda \sim 10$ TeV, which is consistent with the effective interactions with a TeV-scale resonance. Second, we find that in both CP-even and CP-odd cases, the $Z\gamma$ production cross section is about 1-3 fb at the 8 TeV in the allowed parameter space. The current experimental data tells that the (95% C.L.) upper bound on the $Z\gamma$ production in the dilepton channel is given up to the resonance mass of 1.6 TeV while the higher mass reach is limited by statistics [47]. Nevertheless, we expect that the corresponding limit for the 2 TeV resonance would be comparable to the result at the resonance mass of 1.6 TeV in $Z\gamma$ searches or below the existing limit. Therefore, $\sigma(pp \rightarrow Z\gamma) = \mathcal{O}(1)$ fb is still allowed for the 2 TeV and this channel would rather provide an interesting consistency check for ZZ and W^+W^- excesses. As shown in the right panel of Fig. 1, $BR(Z\gamma)$ is comparable to $BR(ZZ)$, and one cannot turn off $BR(Z\gamma)$, as it would also eliminate the signal. In other words, if diboson excesses turned out to be the real signal

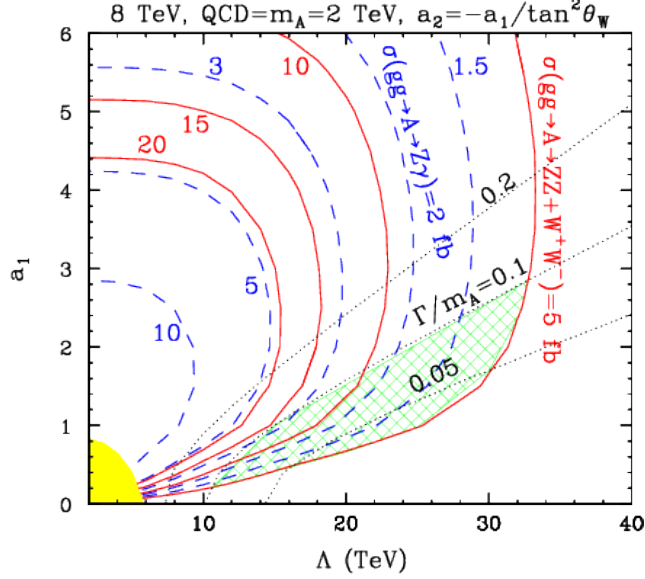


FIG. 2. Same as in Fig. 1 but for CP-odd scalar resonance. Branching fractions are similar to those for the CP-even scalar, replacing s_i by a_i .

with a CP-even or -odd scalar, observation of an excess in the $Z\gamma$ channel would corroborate the case.

III. SPIN-1 RESONANCES

For spin-1 resonances, we consider an extra $U(1)_X$ gauge symmetry that is realized by the Stueckelberg mechanism. Then, the would-be Goldstone boson a_X ensures the gauge invariance of the effective action. Imposing the SM gauge symmetry and $U(1)_X$, we have the dimension-4 interaction Lagrangian between the $U(1)_X$ gauge boson and the quarks and/or gauge bosons in the SM given as follows:

$$\mathcal{L}_{D4} = -g_X Z'_\mu \bar{q} \gamma^\mu (c_L P_L + c_R P_R) q - \frac{1}{2} \epsilon F_{\mu\nu}^Y F^{X\mu\nu} - \left(i\eta D^\mu a_X (H^\dagger D_\mu H) + \text{c.c.} \right), \quad (8)$$

where the covariant derivative is defined as $D_\mu a_X \equiv \partial_\mu a_X - g_X Z'_\mu$ with a_X being the Stueckelberg axion, g_X is the Z' gauge coupling, and $c_R = c_L$ ($c_R = -c_L$) for CP-even (CP-odd) Z' . These dimension-4 interactions correspond to diquark couplings, gauge kinetic mixing and mass mixing in order. We note that in the presence of the Z' gauge couplings to the SM quarks, one has to consider the cancellation of gauge anomalies associated with $U(1)_X$

properly. However, in this work, we simply assume the diquark coupling to be a free parameter, as the detailed model building for consistent Z' gauge couplings is beyond the scope of our work.

It is noteworthy that the interactions of a vector isospin triplet W' to the SM electroweak gauge bosons can be introduced by a similar dimension-4 operator in the effective theory such as $W'_\mu H^\dagger \sigma^a D^\mu H$ [11], which mixes the extra gauge boson with the SM massive gauge bosons. In this case, the ATLAS diboson excesses can be explained by the $W^\pm Z$ channel, provided that the charged spin-1 resonance is produced via quark annihilation at the LHC [11]. In our work, we do not investigate the potential of the charged resonance as mentioned earlier because the dibosonic decays of a neutral resonance suffice to explain the ATLAS diboson excesses within current experimental errors.

Moving onto higher dimensional operators, we enumerate CP-even dimension-6 operators as follows [44]:

$$\begin{aligned} \mathcal{L}_{D6} = & \frac{a_1}{\Lambda^2} D^\mu a_X [i(D^\nu H)^\dagger \tilde{F}_{\mu\nu}^Y H + \text{c.c.}] + \frac{a_2}{\Lambda^2} D^\mu a_X [(D^\nu H)^\dagger F_{\mu\nu}^Y H + \text{c.c.}] \\ & + \frac{a_3}{\Lambda^2} D^\mu a_X [i(D^\nu H)^\dagger \tilde{F}_{\mu\nu}^W H + \text{c.c.}] + \frac{a_4}{\Lambda^2} D^\mu a_X [(D^\nu H)^\dagger F_{\mu\nu}^W H + \text{c.c.}] \\ & + \frac{1}{\Lambda^2} \partial^\mu D_\mu a_X \left(b_1 F_{\rho\sigma}^Y \tilde{F}^{Y\rho\sigma} + b_2 F_{\rho\sigma}^W \tilde{F}^{W\rho\sigma} + b_3 G_{\rho\sigma} \tilde{G}^{\rho\sigma} \right), \end{aligned} \quad (9)$$

where Λ is of order the mass of extra heavy fermions, and a_i ($i = 1, 2, 3, 4$) and b_i ($i = 1, 2, 3$) parametrize the coupling strengths. The CP-odd counterparts of dimension-6 interactions are

$$\begin{aligned} \tilde{\mathcal{L}}_{D6} = & \frac{\tilde{a}_1}{\Lambda^2} D^\mu a_X [i(D^\nu H)^\dagger F_{\mu\nu}^Y H + \text{c.c.}] + \frac{\tilde{a}_2}{\Lambda^2} D^\mu a_X [(D^\nu H)^\dagger \tilde{F}_{\mu\nu}^Y H + \text{c.c.}] \\ & + \frac{\tilde{a}_3}{\Lambda^2} D^\mu a_X [i(D^\nu H)^\dagger F_{\mu\nu}^W H + \text{c.c.}] + \frac{\tilde{a}_4}{\Lambda^2} D^\mu a_X [(D^\nu H)^\dagger \tilde{F}_{\mu\nu}^W H + \text{c.c.}] \\ & + \frac{1}{\Lambda^2} \partial^\mu D_\mu a_X \left(\tilde{b}_1 F_{\rho\sigma}^Y F^{Y\rho\sigma} + \tilde{b}_2 F_{\rho\sigma}^W F^{W\rho\sigma} + \tilde{b}_3 G_{\rho\sigma} G^{\rho\sigma} \right), \end{aligned} \quad (10)$$

where \tilde{a}_i ($i = 1, 2, 3, 4$) and \tilde{b}_i ($i = 1, 2, 3$) parametrize the coupling strengths. We comment on the dimension-6 operators composed of one field strength tensor for Z' and two field strength tensors for the SM gauge bosons: $\text{Tr}(F_\mu^{X\lambda} F_{\lambda\nu} \tilde{F}^{\nu\mu})$ for CP-even operators and $\text{Tr}(F_\mu^{X\lambda} F_{\lambda\nu} F^{\nu\mu})$ for CP-odd operators with $F_{\mu\nu} = F_{\mu\nu}^Y, F_{\mu\nu}^W, G_{\mu\nu}$. First of all, the CP-odd operators can be rewritten as $F_\mu^{X\nu} F_{\nu\lambda} F^{\lambda\mu} = F_{\mu\nu}^X F_{\lambda\nu} F^{\mu\lambda}$, which is the same as $F_{\nu\mu}^X F_{\lambda\nu} F^{\mu\lambda} = -F_{\mu\nu}^X F_{\lambda\nu} F^{\mu\lambda}$, and as a result, we get $F_\mu^{X\nu} F_{\nu\lambda} F^{\lambda\mu} = 0$. Likewise, the CP-even operators can be also rewritten as $F_\mu^{X\nu} F_{\nu\lambda} \tilde{F}^{\lambda\mu} = F_{\mu\nu}^X F_{\lambda\nu} \tilde{F}^{\mu\lambda}$. Then, using the identity

of $F_{\lambda\mu}\tilde{F}^{\nu\lambda} = -\frac{1}{4}\delta_\mu^\nu F_{\alpha\beta}\tilde{F}^{\alpha\beta}$, we get $F_\mu^{X\nu}F_{\nu\lambda}\tilde{F}^{\lambda\mu} = -\frac{1}{4}F_\mu^{X\mu}F_{\alpha\beta}\tilde{F}^{\alpha\beta} = 0$. Therefore, the dimension-6 operators composed of gauge field strength tensors only are identically zero so that we do not consider them in our analysis.

Given the above observations, the Z' gauge boson decays only by symmetry breaking terms given in \mathcal{L}_{D6} or $\tilde{\mathcal{L}}_{D6}$. When it comes to the production modes for the spin-1 resonance, we henceforth assume that it is produced by diquark couplings and ignore the gauge kinetic mixing and mass mixing. The effective cubic interactions for Z' coming from \mathcal{L}_{D6} and $\tilde{\mathcal{L}}_{D6}$ are obtained as shown below:

$$\begin{aligned}\mathcal{L}_{\text{CP-even}} = & \frac{v}{\Lambda^2} \left(a_1 m_Z Z^\nu Z'^\mu \tilde{F}_{\mu\nu}^Y + a_2 \partial^\nu h Z'^\mu F_{\mu\nu}^Y \right) \\ & - \frac{v}{\Lambda^2} \left(\frac{1}{2} a_3 m_Z \epsilon^{\mu\nu\rho\sigma} Z_\nu Z'_\mu (\partial_\rho W_\sigma^3 - \partial_\sigma W_\rho^3) + a_4 \partial^\nu h Z'^\mu (\partial_\mu W_\nu^3 - \partial_\nu W_\mu^3) \right) \\ & + \frac{m_W v}{\Lambda^2} Z'_\mu \left(-\frac{1}{2} a_3 \epsilon^{\mu\nu\rho\sigma} W_\nu^- (\partial_\rho W_\sigma^+ - \partial_\sigma W_\rho^+) + i a_4 W^{-\nu} (\partial_\mu W_\nu^+ - \partial_\nu W_\mu^+) + \text{c.c.} \right) \\ & + \frac{1}{\Lambda^2} \partial^\mu Z'_\mu \left(b_1 F_{\rho\sigma}^Y \tilde{F}^{Y\rho\sigma} + b_2 F_{\rho\sigma}^W \tilde{F}^{W\rho\sigma} + b_3 G_{\rho\sigma} \tilde{G}^{\rho\sigma} \right),\end{aligned}\quad (11)$$

$$\begin{aligned}\mathcal{L}_{\text{CP-odd}} = & \frac{v}{\Lambda^2} \left(\tilde{a}_1 m_Z Z^\nu Z'^\mu F_{\mu\nu}^Y + \tilde{a}_2 \partial^\nu h Z'^\mu \tilde{F}_{\mu\nu}^Y \right) \\ & - \frac{v}{\Lambda^2} \left(\tilde{a}_3 m_Z Z^\nu Z'^\mu (\partial_\mu W_\nu^3 - \partial_\nu W_\mu^3) + \frac{1}{2} \tilde{a}_4 \epsilon^{\mu\nu\rho\sigma} \partial_\nu h Z'_\mu (\partial_\rho W_\sigma^3 - \partial_\sigma W_\rho^3) \right) \\ & + \frac{m_W v}{\Lambda^2} Z'_\mu \left(-\tilde{a}_3 W_\nu^- (\partial^\mu W^{+\nu} - \partial^\nu W^{+\mu}) + \frac{1}{2} i \tilde{a}_4 \epsilon^{\mu\nu\rho\sigma} W_\nu^- (\partial_\rho W_\sigma^+ - \partial_\sigma W_\rho^+) + \text{c.c.} \right) \\ & + \frac{1}{\Lambda^2} \partial^\mu Z'_\mu \left(\tilde{b}_1 F_{\rho\sigma}^Y F^{Y\rho\sigma} + \tilde{b}_2 F_{\rho\sigma}^W F^{W\rho\sigma} + \tilde{b}_3 G_{\rho\sigma} G^{\rho\sigma} \right),\end{aligned}\quad (12)$$

where the $U(1)_X$ gauge coupling is absorbed into a_1 and \tilde{a}_1 , and so on.

After the electroweak symmetry breaking (EWSB) and dropping the terms with the divergence of Z' , the effective CP-even interactions for Z' are

$$\begin{aligned}\mathcal{L}_{\text{CP-even}} = & \kappa_1 \epsilon^{\mu\nu\rho\sigma} Z'_\mu Z_\nu F_{\rho\sigma} + \hat{\kappa}_1 \epsilon^{\mu\nu\rho\sigma} Z'_\mu Z_\nu (\partial_\rho Z_\sigma - \partial_\sigma Z_\rho) \\ & + \left(\kappa_2 \epsilon^{\mu\nu\rho\sigma} Z'_\mu W_\nu^- (\partial_\rho W_\sigma^+ - \partial_\sigma W_\rho^+) + i \hat{\kappa}_2 Z'^\mu W^{-\nu} (\partial_\mu W_\nu^+ - \partial_\nu W_\mu^+) + \text{c.c.} \right) \\ & + \frac{\kappa_3}{\Lambda} Z'^\mu \partial^\nu h F_{\mu\nu} + \frac{\hat{\kappa}_3}{\Lambda} Z'^\mu \partial^\nu h (\partial_\mu Z_\nu - \partial_\nu Z_\mu)\end{aligned}\quad (13)$$

where $F_{\mu\nu}$ is the photon field strength tensor and $\kappa_2, \hat{\kappa}_2$ are related to other parameters by gauge invariance as

$$\kappa_2 = \frac{m_W}{m_Z} \left(\kappa_1 \sin \theta_W + \hat{\kappa}_1 \cos \theta_W \right), \quad \hat{\kappa}_2 = -\frac{m_W}{\Lambda} \left(\kappa_3 \sin \theta_W + \hat{\kappa}_3 \cos \theta_W \right).\quad (14)$$

We note that the effective triple gauge interactions with Z' in the above effective Lagrangian are the generalized Chern-Simons terms that are generated by extra heavy fermions [42, 44]. Using the effective action above, we obtain the partial decay rates of the spin-1 resonance [42] into $Z\gamma$, ZZ , W^+W^- , $h\gamma$, hZ , and $q\bar{q}$, respectively as:

$$\left\{ \begin{array}{l} \Gamma_{Z'}(Z\gamma) = \frac{\kappa_1^2 m_{Z'}^3}{24\pi m_Z^2} (1 - x_Z^{Z'})^3 (1 + x_Z^{Z'}), \\ \Gamma_{Z'}(ZZ) = \frac{\hat{\kappa}_1^2 m_{Z'}^3}{24\pi m_Z^2} (1 - 4x_Z^{Z'})^{5/2}, \\ \Gamma_{Z'}(W^+W^-) = \frac{m_{Z'}^3 (1 - 4x_W^{Z'})^{3/2}}{48\pi m_W^2} [4\kappa_2^2 (1 - 4x_W^{Z'}) + \hat{\kappa}_2^2 (1 + 3x_W^{Z'})], \\ \Gamma_{Z'}(h\gamma) = \frac{\kappa_3^2 m_{Z'}^3}{96\pi \Lambda^2} (1 - x_h^{Z'})^3, \\ \Gamma_{Z'}(hZ) = \frac{\hat{\kappa}_3^2 m_{Z'}^3}{192\pi \Lambda^2} \left(1 - (\sqrt{x_h^{Z'}} + \sqrt{x_Z^{Z'}})^2\right)^{1/2} \left(1 - (\sqrt{x_h^{Z'}} - \sqrt{x_Z^{Z'}})^2\right)^{1/2} \\ \quad \times (2 + x_Z^{Z'}(x_h^{Z'} - x_Z^{Z'})^2 + 2x_h^{Z'}(x_h^{Z'} + 3x_Z^{Z'}) - (4x_h^{Z'} + 3x_Z^{Z'})), \\ \Gamma_{Z'}(q\bar{q}) = \frac{g_X^2 m_{Z'}}{4\pi} (1 + 2x_q^{Z'}) (1 - 4x_q^{Z'})^{1/2}, \end{array} \right. \quad (15)$$

where $x_i^{Z'}$ is defined in Eq. (3). On the other hand, the effective CP-odd interactions for Z' become

$$\begin{aligned} \mathcal{L}_{\text{CP-odd}} = & \alpha_1 Z'^\mu Z^\nu F_{\mu\nu} + \hat{\alpha}_1 Z'^\mu Z^\nu (\partial_\mu Z_\nu - \partial_\nu Z_\mu) \\ & + \left(\alpha_2 Z'^\mu W^{-\nu} (\partial_\mu W_\nu^+ - \partial_\nu W_\mu^+) + i\hat{\alpha}_2 \epsilon^{\mu\nu\rho\sigma} Z'_\mu W_\nu^- (\partial_\rho W_\sigma^+ - \partial_\sigma W_\rho^+) + \text{c.c.} \right) \\ & + \frac{\alpha_3}{\Lambda} \epsilon^{\mu\nu\rho\sigma} Z'_\mu \partial_\nu h F_{\rho\sigma} + \frac{\hat{\alpha}_3}{\Lambda} \epsilon^{\mu\nu\rho\sigma} Z'_\mu \partial_\nu h (\partial_\rho Z_\sigma - \partial_\sigma Z_\rho), \end{aligned} \quad (16)$$

where $\alpha_2, \hat{\alpha}_2$ are related to other parameters by gauge invariance as

$$\alpha_2 = \frac{m_W}{m_Z} (\alpha_1 \sin \theta_W + \hat{\alpha}_1 \cos \theta_W), \quad \hat{\alpha}_2 = -\frac{m_W}{\Lambda} (\alpha_3 \sin \theta_W + \hat{\alpha}_3 \cos \theta_W). \quad (17)$$

The partial decay widths of the CP-odd vector into $Z\gamma$, ZZ , W^+W^- , $h\gamma$, hZ , and $q\bar{q}$, respectively are given as follows:

$$\left\{ \begin{array}{l} \Gamma_{Z'}(Z\gamma) = \frac{\alpha_1^2 m_{Z'}^3}{96\pi m_Z^2} (1 - x_Z^{Z'})^3 (1 + x_Z^{Z'}), \\ \Gamma_{Z'}(ZZ) = \frac{\hat{\alpha}_1^2 m_{Z'}^3}{96\pi m_Z^2} (1 - 4x_Z^{Z'})^{3/2}, \\ \Gamma_{Z'}(W^+W^-) = \frac{m_{Z'}^3 \sqrt{1 - 4x_W^{Z'}}}{48\pi m_W^2} [\alpha_2^2 (1 - 4x_W^{Z'}) + 4\hat{\alpha}_2^2 (1 + 2x_W^{Z'})], \\ \Gamma_{Z'}(h\gamma) = \frac{\alpha_3^2 m_{Z'}^3}{24\pi \Lambda^2} (1 - x_h^{Z'})^3, \\ \Gamma_{Z'}(hZ) = \frac{\hat{\alpha}_3^2 m_{Z'}^3}{24\pi \Lambda^2} \left(1 - (\sqrt{x_h^{Z'}} + \sqrt{x_Z^{Z'}})^2\right)^{3/2} \left(1 - (\sqrt{x_h^{Z'}} - \sqrt{x_Z^{Z'}})^2\right)^{3/2}, \\ \Gamma_{Z'}(q\bar{q}) = \frac{g_X^2 m_{Z'}}{4\pi} (1 - 4x_q^{Z'})^{3/2}. \end{array} \right. \quad (18)$$

As can be seen clearly from the gauge invariant higher dimensional operators in Eqs. (9) and (10) and can be checked from the effective gauge interactions in Eqs. (13) and (16), we note that the unitarity cutoff of $\Lambda \sim 10$ TeV, implies that $\kappa_{1,2}, \hat{\kappa}_{1,2}, \alpha_{1,2}, \hat{\alpha}_{1,2} \lesssim \mathcal{O}(10^{-2})$ and $\kappa_3, \alpha_3 \lesssim \mathcal{O}(1)$.

For a phenomenological study of the spin-1 resonance, we assume that the higher dimensional operators given in Eqs. (11) and (12) come with pure imaginary coefficients, i.e. $a_2 = a_4 = 0$ and $\tilde{a}_2 = \tilde{a}_4 = 0$. Then, we get

$$\kappa_3 = \hat{\kappa}_3 = 0, \quad \tilde{\kappa}_2 = 0, \quad \kappa_2 = \frac{m_W}{m_Z} (\kappa_1 \sin \theta_W + \hat{\kappa}_1 \cos \theta_W), \quad (19)$$

for CP-even interactions, and, similarly,

$$\alpha_3 = \hat{\alpha}_3 = 0, \quad \hat{\alpha}_2 = 0, \quad \alpha_2 = \frac{m_W}{m_Z} (\alpha_1 \sin \theta_W + \hat{\alpha}_1 \cos \theta_W), \quad (20)$$

for CP-odd interactions. There are two free parameters for SM gauge boson couplings in each case, $\kappa_1, \hat{\kappa}_1$ and $\alpha_1, \hat{\alpha}_1$, respectively. In this case, there are no $h\gamma$ or hZ decay modes of the Z' gauge boson while $Z\gamma, ZZ$ and W^+W^- decay modes exist. Therefore, the gauge invariance of the higher dimensional operators is crucial in correlating between different decay channels of the spin-1 resonance. Turning on small couplings to Higgs, we can maintain the diboson resonances as hinted by ATLAS and at the same time have a potential to discover or constrain the models with spin-1 resonance further by the decay mode into $h\gamma$ or hZ . Henceforth, in order to explain the ATLAS diboson excess from W^+W^- and ZZ decay modes, we focus on a simple parameter choice with $\kappa_3 = \hat{\kappa}_3 = 0$ for the CP-even and $\alpha_3 = \hat{\alpha}_3 = 0$ for the CP-odd. In this case, the ratio between W^+W^- and ZZ branching fractions remains constant, independent of the remaining parameters for both cases, i.e., $\frac{BR(Z' \rightarrow W^+W^-)}{R(Z' \rightarrow ZZ)} \approx 1.56$. In Fig. 3, we show branching fractions of the CP-even vector as a function of the diquark coupling (g_X) for above choice of parameters. In addition, we have fixed $\hat{\kappa}_1 = 0.01$ (considering the unitarity bound) to maximize the branching fraction into W^+W^- and ZZ , as their partial decays widths are proportional to $\hat{\kappa}_1^2$ for $\kappa_1 = \kappa_3 = \hat{\kappa}_3 = b_i = 0$. Numerically very similar results are obtained for the CP-odd vector.

For our numerical study, we set $c_L = c_R = 1$ for the CP-even ($-c_L = c_R = 1$ for the CP odd) and ignore the kinetic mixing and mass mixing. We further set $b_i = 0$ for the CP-even case ($\tilde{b}_i = 0$ for the CP-odd case), leaving $\kappa_1, \hat{\kappa}_1, \kappa_3, \hat{\kappa}_3, \Lambda$ and g_X for the CP-even, and $\alpha_1, \hat{\alpha}_1, \alpha_3, \hat{\alpha}_3, \Lambda$ and g_X for the CP-odd, respectively, as relevant parameters. Dependence

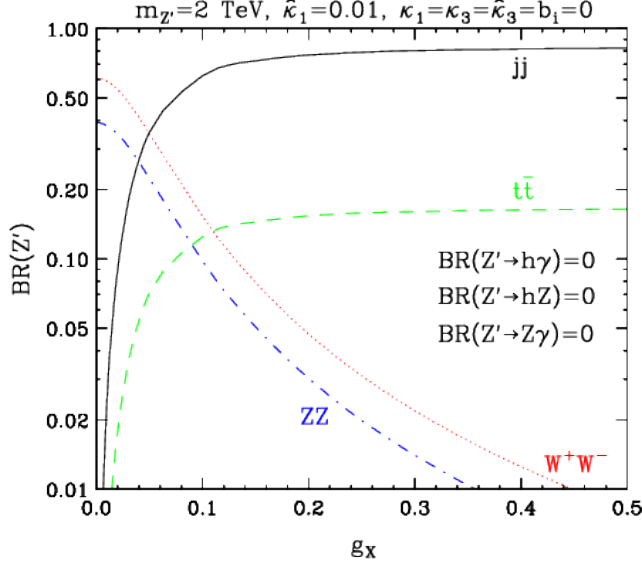


FIG. 3. Branching fractions of the CP-even vector as a function of g_X (diquark coupling) for a given set of parameters, $\hat{\kappa}_1 = 0.01$ and $\kappa_1 = \kappa_3 = \hat{\kappa}_3 = b_i = 0$. Very similar results are obtained for the CP-odd vector and the CP-odd tensor cases.

on κ_3 , $\hat{\kappa}_3$, α_3 and $\hat{\alpha}_3$ are weak, and we set them to zero as mentioned above to make $\sigma(h\gamma)$ and $\sigma(hZ)$ vanish. Furthermore, we conservatively take $\kappa_1 = 0 = \alpha_1$, for which $\sigma(Z\gamma)$ also vanishes. Turning on non-zero values of κ_1 and α_1 always reduces the branching fractions of the diboson signal. Finally, after setting $\Lambda = 10$ TeV, we show in Fig. 4 the production cross sections of the CP-even (left panel) and the CP-odd (right panel) vector bosons in the $ZZ + W^+W^-$ final state (red solid curves). As the resonance is produced by pp collision, it can also decays to the dijet final state. The dark yellow-shaded area is disfavored by ATLAS dijet searches [40] and the black dotted curves represent $\Gamma_{Z'}/m_{Z'} = 0.15$, 0.1, and 0.05, respectively.

The single production cross section itself is explicitly dependent on the coupling, g_X , only. However, the decay width changes depending on the rest of parameters, which affect the shape of the dijet cross section. Our CP-even vector model is the same as one in discussed in Ref. [48], and we are able to use results there by simply rescaling couplings and branching fractions in our parameter space. The blue (solid, dashed, dotted) curves labelled by 10 fb^{-1} , 300 fb^{-1} , and 3 ab^{-1} represent the projected 95% C.L. exclusion contours for 14 TeV LHC, respectively. Unfortunately, this projected sensitivity is not available for other resonances,

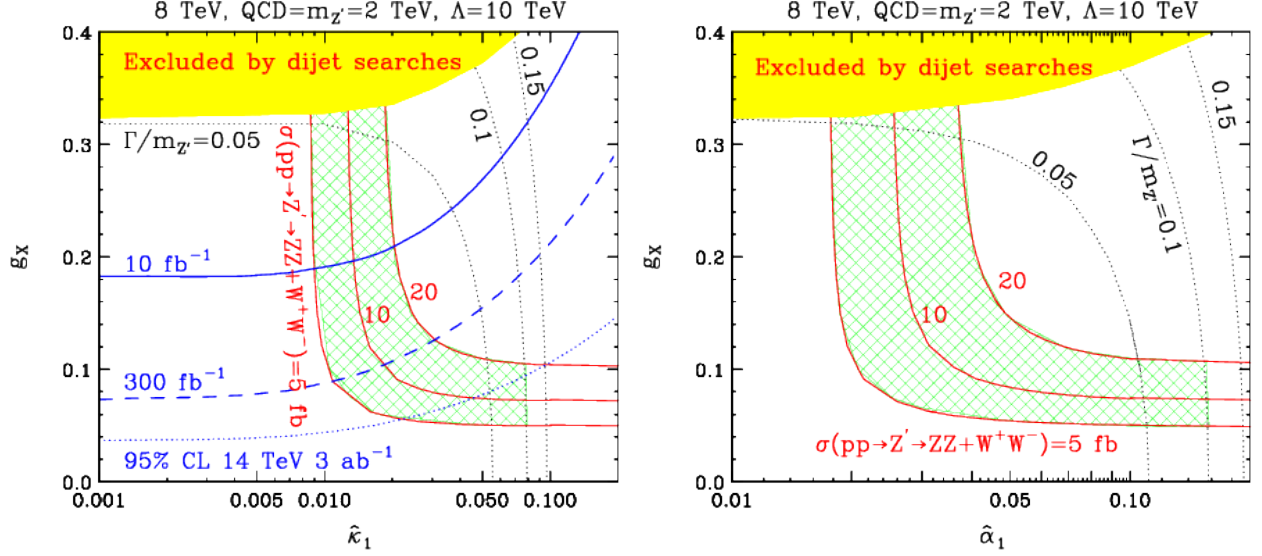


FIG. 4. Production cross sections (in fb) of the CP-even (left panel) and the CP-odd (right panel) vector bosons in the $ZZ + W^+W^-$ final state. The dark yellow-shaded region is disfavored by ATLAS dijet searches and the black dotted curves represent $\Gamma_{Z'}/m_{Z'} = 0.15, 0.1,$ and $0.05,$ respectively. The light green-shaded region represents the allowed space to fit the ATLAS diboson data. The blue (solid, dashed, dotted) curves represent the projected 95% C.L. exclusion contours for 14 TeV LHC with the corresponding luminosity.

and it is not straightforward to recast the results from Ref. [48] due to different efficiencies.

We note that as shown in the right panel of Fig. 4, the allowed parameter space requires $\hat{\alpha}_1 \gtrsim 0.02,$ which is close to the unitarity limit. Finally, any reasonable deviation from the current choice of parameters would be easily allowed, as long as the corresponding limits can be avoided in the final states with $Z\gamma, hZ,$ and $h\gamma.$

IV. SPIN-2 RESONANCES

The spin-2 resonance $\mathcal{G}_{\mu\nu}$ with mass m_G couples to the SM particles as graviton does, that is,

$$\mathcal{L}_{\text{CP-even}}^{\mathcal{G}} = \frac{1}{\Lambda} \mathcal{G}_{\mu\nu} T^{\mu\nu}, \quad (21)$$

where $T_{\mu\nu}$ is the energy-momentum tensor. For CP-even interactions, we set the spin-2 resonance to couple to the energy-momentum tensor for each SM particle with an arbitrary

coefficient, which is gauge invariant under the SM gauge groups. The energy-momentum tensor with CP-even interactions to the SM gauge bosons are

$$T_{\mu\nu} = c_1 F_{\mu\lambda}^Y F^{Y\lambda}{}_{\nu} + c_2 F_{\mu\lambda}^W F^{W\lambda}{}_{\nu} + c_3 G_{\mu\lambda} G^{\lambda}{}_{\nu}, \quad (22)$$

where c_1 , c_2 , and c_3 are constant coefficients parametrizing the relevant coupling strengths. Here, we assumed that the spin-2 resonance couples dominantly to the transverse modes of SM gauge bosons [43] while the terms proportional to the metric $g_{\mu\nu}$ in the energy-momentum tensor vanish under the traceless condition. For a heavy spin-2 resonance with $m_G \gg m_{W,Z}$, the gauge boson mass terms can be ignored, even if the spin-2 resonance couples to the longitudinal modes of gauge bosons as well [43].

The partial decay widths of the spin-2 resonance with CP-even interactions into $\gamma\gamma$, $Z\gamma$, ZZ , W^+W^- , and gg [43] are

$$\left\{ \begin{array}{ll} \Gamma_{\mathcal{G}}(\gamma\gamma) = \frac{|c_{\gamma\gamma}|^2 m_G^3}{80\pi\Lambda^2}, & c_{\gamma\gamma} = c_1 \cos^2 \theta_W + c_2 \sin^2 \theta_W \\ \Gamma_{\mathcal{G}}(Z\gamma) = \frac{|c_{\gamma Z}|^2 m_G^3}{160\pi\Lambda^2} (1 - x_Z^G)^3 (1 + \frac{1}{2}x_Z^G + \frac{1}{6}(x_Z^G)^2), & c_{Z\gamma} = (c_2 - c_1) \sin(2\theta_W) \\ \Gamma_{\mathcal{G}}(ZZ) = \frac{|c_{ZZ}|^2 m_G^3}{80\pi\Lambda^2} \sqrt{1 - 4x_Z^G} (1 - 3x_Z^G + 6(x_Z^G)^2), & c_{ZZ} = c_2 \cos^2 \theta_W + c_1 \sin^2 \theta_W \\ \Gamma_{\mathcal{G}}(W^+W^-) = \frac{|c_{WW}|^2 m_G^3}{160\pi\Lambda^2} \sqrt{1 - 4x_W^G} (1 - 3x_W^G + 6(x_W^G)^2), & c_{WW} = 2c_2 \\ \Gamma_{\mathcal{G}}(gg) = \frac{|c_{gg}|^2 m_G^3}{10\pi\Lambda^2}, & c_{gg} = c_3, \end{array} \right. \quad (23)$$

where again x_i^G is defined in Eq. (3). One may notice that for $c_1 = c_2$, the decay mode, $\mathcal{G} \rightarrow Z\gamma$, vanishes. We note that the branching fractions of the spin-2 resonance are of the similar form as the ones of scalar resonances discussed in Section II because the spin-2 resonance decays through gauge invariant operators composed of field strength tensors. One can also suppress the diphoton rate by choosing $c_2 = -c_1/\tan^2 \theta_W$, which forces all relevant branching fractions to be the same as those in the scalar case. Our parameter scan results are summarized in Fig. 5. We also find that production cross section, $gg \rightarrow \mathcal{G} \rightarrow gg$, in the demonstrated parameter space was small and therefore, there is no constraint from the LHC dijet resonance search.

On the other hand, there is no counterpart of the energy-momentum tensor for CP-odd interactions, but the Lorentz invariance and the gauge invariance dictate the detailed form of the interactions. Following the similar step as in the CP-even vector case, the CP-odd

interactions of the spin-2 resonance to the SM gauge bosons² are given by

$$\mathcal{L}_{\text{CP-odd}}^{\mathcal{G}} = \frac{1}{\Lambda} \mathcal{G}_{\mu\nu} \tilde{T}^{\mu\nu}, \quad (24)$$

where $\tilde{T}_{\mu\nu} = \tilde{T}_{1,\mu\nu} + \tilde{T}_{2,\mu\nu}$ with

$$\begin{aligned} \tilde{T}_{1,\mu\nu} = & a_1 \epsilon_{\mu\lambda\rho\sigma} \partial^\lambda Z_\nu F^{\rho\sigma} + \hat{a}_1 \epsilon_{\mu\lambda\rho\sigma} \partial^\lambda Z_\nu (\partial^\rho Z^\sigma - \partial^\sigma Z^\rho) \\ & + \left(a_2 \epsilon_{\mu\lambda\rho\sigma} \partial^\lambda W_\nu^- (\partial^\rho W^{\sigma+} - \partial^\sigma W^{\rho+}) + i \hat{a}_2 \partial^\lambda W_\nu^- (\partial_\mu W_\lambda^+ - \partial_\lambda W_\mu^+) + \text{c.c.} \right) \\ & + \frac{a_3}{\Lambda} \partial^\lambda \partial_\nu h F_{\mu\lambda} + \frac{\hat{a}_3}{\Lambda} \partial^\lambda \partial_\nu h (\partial_\mu Z_\lambda - \partial_\lambda Z_\mu), \end{aligned} \quad (25)$$

$$\tilde{T}_{2,\mu\nu} = \frac{i}{2} a_q \bar{q} \gamma^5 (\gamma^\mu \partial^\nu + \gamma^\nu \partial^\mu) q - \frac{i}{2} a_q ((\partial^\mu \bar{q}) \gamma^5 \gamma^\nu + (\partial^\nu \bar{q}) \gamma^5 \gamma^\mu) q. \quad (26)$$

Here a_2 and \hat{a}_2 are related to other parameters through gauge invariance as

$$a_2 = \frac{m_W}{m_Z} \left(a_1 \sin \theta_W + \hat{a}_1 \cos \theta_W \right), \quad \hat{a}_2 = -\frac{m_W}{\Lambda} \left(a_3 \sin \theta_W + \hat{a}_3 \cos \theta_W \right). \quad (27)$$

The operators in $\tilde{T}_{1,\mu\nu}$ are induced from higher dimensional gauge-invariant operators such as $[D^\lambda D_\nu H]^\dagger \tilde{F}_{\mu\lambda}^Y H$, $[D^\lambda D_\nu H]^\dagger F_{\mu\lambda}^Y H$, $[D^\lambda D_\nu H]^\dagger \tilde{F}_{\mu\lambda}^W H$, and $[D^\lambda D_\nu H]^\dagger F_{\mu\lambda}^W H$ after electroweak symmetry breaking.³ Therefore, the resulting effective CP-odd interactions of the spin-2 resonance are of strong similarity to those of the spin-1 resonances as discussed in Section III. Hence, the spin-2 resonance can decay into a pair of electroweak gauge bosons or Higgs bosons via symmetry breaking terms in $\tilde{T}_{1,\mu\nu}$. On the other hand, diquark CP-odd operators in $\tilde{T}_{2,\mu\nu}$ lead to the production of the CP-odd spin-2 resonance. We note that as in the CP-odd vector case, the unitarity cutoff of $\Lambda \sim 10 \text{ TeV}$ implies that $a_{1,2}$, $\hat{a}_{1,2} \lesssim \mathcal{O}(10^{-2})$ and a_3 , $\hat{a}_3 \lesssim \mathcal{O}(1)$.

We remark that the operators composed of field strength tensors only, for example, $\mathcal{G}_{\mu\nu} \text{Tr}(\tilde{F}_{\mu\lambda} F^\lambda{}_\nu)$ with $F_{\mu\nu}$ being $F_{\mu\nu}^Y$, $F_{\mu\nu}^W$, or $G_{\mu\nu}$, vanish because $\mathcal{G}_{\mu\nu} \text{Tr}(\tilde{F}_{\mu\lambda} F^\lambda{}_\nu) = -\frac{1}{4} \mathcal{G}_\mu^\mu \text{Tr}(F_{\alpha\beta} \tilde{F}^{\alpha\beta}) = 0$ due to the traceless condition, i.e., $\mathcal{G}_\mu^\mu = 0$. Therefore, those gauge invariant operators do not contribute to the process with on-shell CP-odd tensor so that we do not consider them in our analysis.

² The ZZ coupling to the CP-odd tensor field was considered in Ref. [46] without gauge invariance imposed.

³ We note that one of higher dimensional operators among $[D_\nu D^\lambda H]^\dagger \tilde{F}_{\mu\lambda}^Y H$ and $[D^\lambda D_\nu H]^\dagger \tilde{F}_{\mu\lambda}^Y H$ is redundant because $[D^\lambda D_\nu H - D_\nu D^\lambda H]^\dagger \tilde{F}_{\mu\lambda}^Y H \sim |H|^2 F^{Y\lambda}{}_\nu \tilde{F}_{\mu\lambda}^Y$, which contributes to the gauge invariant operators of $F^{Y\lambda}{}_\nu \tilde{F}_{\mu\lambda}^Y$ that becomes a vanishing gauge interaction after electroweak symmetry breaking (EWSB).

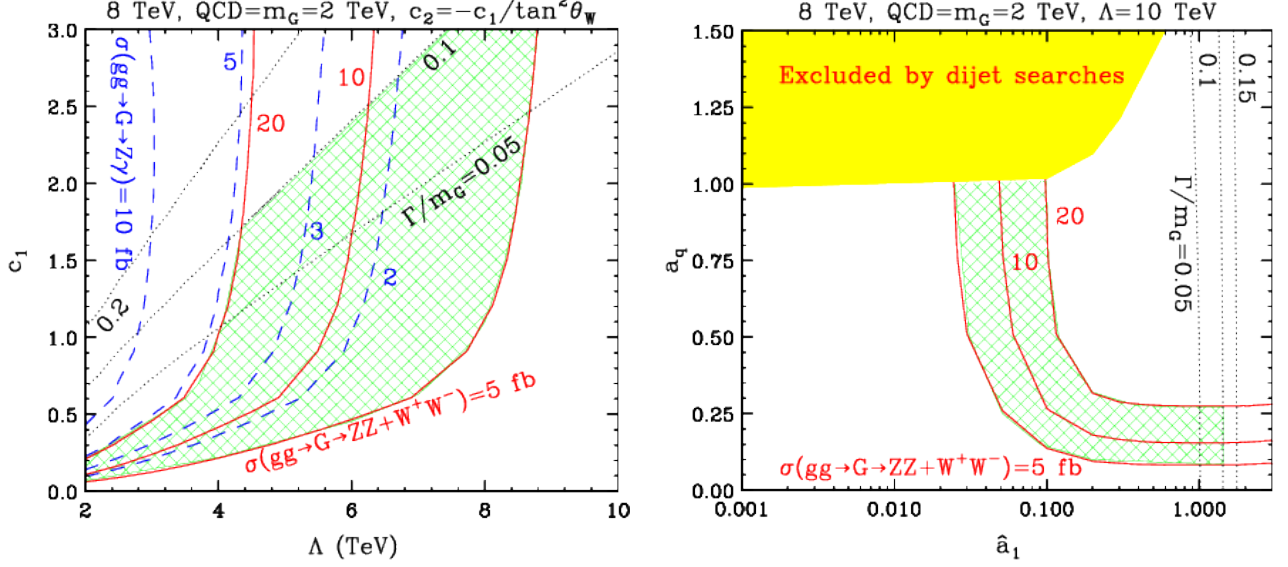


FIG. 5. Similar to Fig. 4 but for the CP-even tensor (left panel) and the CP-odd tensor (right panel). For the CP-even tensor, branching fractions are similar to those for the CP-even scalar, replacing s_i by c_i .

The partial decay rates with CP-odd interactions into $Z\gamma$, ZZ , W^+W^- , $h\gamma$, hZ and $q\bar{q}$ are listed below:

$$\left\{ \begin{array}{l}
 \Gamma_G(Z\gamma) = \frac{a_1^2 m_G^3}{960\pi\Lambda^2} (1 - x_Z^G)^3 (34 + 3x_Z^G + 3(x_Z^G)^{-1}), \\
 \Gamma_G(ZZ) = \frac{\hat{a}_1^2 m_G^5}{960\pi m_Z^2 \Lambda^2} \sqrt{1 - 4x_Z^G} (3 - 4x_Z^G - 32(x_Z^G)^2), \\
 \Gamma_G(W^+W^-) = \frac{m_G^5}{1920\pi m_W^2 \Lambda^2} (1 - 4x_W^G)^{3/2} [3\hat{a}_2^2 (1 - 4x_W^G) + 4a_2^2 (3 + 8x_W^G)], \\
 \Gamma_G(h\gamma) = \frac{a_3^2 m_G^5}{1280\pi\Lambda^4} (1 - x_h^G)^5, \\
 \Gamma_G(hZ) = \frac{\hat{a}_3^2 m_G^5}{3840\pi\Lambda^4} \left[(1 - x_h^G)^2 - 2(1 + x_Z^G)x_Z^G + (x_Z^G)^2 \right]^{5/2} \\
 \quad \times \left[3(1 - x_Z^G)^2 + 2(-2 + 5x_h^G + (x_h^G)^2)x_Z^G - (1 + 4x_h^G)(x_Z^G)^2 + 2(x_Z^G)^3 \right] \\
 \quad \approx \frac{\hat{a}_3^2 m_G^5}{1280\pi\Lambda^4}, \\
 \Gamma_G(q\bar{q}) = \frac{3a_q^2 m_G^3}{40\pi\Lambda^2} (1 - x_q^G)^{5/2},
 \end{array} \right. \quad (28)$$

where again x_i^G is defined in Eq. (3).

For a phenomenological study of the CP-odd tensor field, we assume that the higher dimensional operators like $[D^\lambda D_\nu H]^\dagger \tilde{F}_{\mu\lambda}^Y H$ and $[D^\lambda D_\nu H]^\dagger \tilde{F}_{\mu\lambda}^W H$ come with pure imaginary coefficients. We then end up with

$$a_3 = \hat{a}_3 = 0, \quad \hat{a}_2 = 0, \quad a_2 = \frac{m_W}{m_Z} (a_1 \sin\theta_W + \hat{a}_1 \cos\theta_W), \quad (29)$$

from which one can see that there are no $h\gamma$ and hZ decay modes of the CP-odd tensor field but $Z\gamma$, ZZ , and W^+W^- decay channels still remain open.

Furthermore, for the purpose of fitting diboson data, it is more convenient to enhance branching fractions into ZZ and W^+W^- . As the partial decay width of $\mathcal{G} \rightarrow Z\gamma$ is proportional to a_1 , we set a_1 to be zero and examine whether there exists an allowed parameter space. In this set-up, allowed decay modes are ZZ , W^+W^- , jj , and $t\bar{t}$, and parameters \hat{a}_1 and a_q remain free. The Λ does not play a role, as the two parameters can be rescaled. The resulting branching fractions resembles those for the vector resonances as shown in Fig. 3. Our results are shown in the right panel of Fig. 5 for the CP-odd case. In this case, we find that $0.02 \lesssim \hat{a}_1$. Turning on any of other diboson final states hZ , $h\gamma$ and $Z\gamma$ would push this bound on \hat{a}_1 to a higher value, as the branching fraction of $W^+W^- + ZZ$ is reduced. Therefore our study indicates that the CP-odd tensor might have a mild tension between ATLAS diboson data and the unitarity bounds.

V. KINEMATIC CORRELATIONS IN THE DIBOSON FINAL STATE

In this section, we discuss ways of discriminating potential scenarios to give rise to diboson resonances. Since we have observed that various bosonic particles with different spins and CP states can accommodate the excesses reported by the ATLAS collaboration with a suitable choice of parameters, it is of paramount importance to pin down the underlying physics once those excesses are confirmed experimentally. Of potentially useful variables, we employ several angular correlations between the decay products of the resonance of interest. We first suppose that a resonance R decays into two vector bosons V_1 and V_2 which subsequently decay into two visible particles u_i and v_i ($i = 1, 2$):

$$pp \rightarrow R \rightarrow V_1(\rightarrow u_1 + v_1) + V_2(\rightarrow u_2 + v_2), \quad (30)$$

and denote \vec{P}_i as the three momentum of V_i and $\vec{u}_i(\vec{v}_i)$ as those of $u_i(v_i)$.

Scenario	Parameter choice	R production
0^+	$s_1 = 0.4, s_2 = -s_1/\tan^2\theta_W, s_3 = 1, \Lambda = 10 \text{ TeV}$	$gg \rightarrow R$
0^-	$a_1 = 0.6, a_2 = -a_1/\tan^2\theta_W, a_3 = 1, \Lambda = 20 \text{ TeV}$	$gg \rightarrow R$
1^+	$\hat{\kappa}_1 = 0.008, g_X = 0.02, c_L = c_R = 1, \Lambda = 10 \text{ TeV}$	$q\bar{q} \rightarrow R$
1^-	$\hat{\alpha}_1 = 0.01, g_X = 0.04, -c_L = c_R = 1, \Lambda = 10 \text{ TeV}$	$q\bar{q} \rightarrow R$
2^+	$c_1 = 0.5, c_2 = -c_1/\tan^2\theta_W, c_3 = 1, \Lambda = 5 \text{ TeV}$	$gg \rightarrow R$
2^-	$\hat{a}_1 = 0.1, a_q = 0.25, \Lambda = 10 \text{ TeV}$	$q\bar{q} \rightarrow R$

TABLE I. List of scenario choices for a resonance R having a spin and CP-state denoted as J^{CP} .

With these notations, we enumerate the angular variables to be used here as follows:

$$\Phi = \frac{\vec{P}_1 \cdot (\hat{n}_1 \times \hat{n}_2)}{|\vec{P}_1 \cdot (\hat{n}_1 \times \hat{n}_2)|} \cos^{-1}(\hat{n}_1 \cdot \hat{n}_2) \text{ with } \hat{n}_i = \frac{\vec{u}_i \times \vec{v}_i}{|\vec{u}_i \times \vec{v}_i|}, \quad (31)$$

$$\Phi_1 = \frac{\vec{P}_1 \cdot (\hat{n}_1 \times \hat{n}_{sc})}{|\vec{P}_1 \cdot (\hat{n}_1 \times \hat{n}_{sc})|} \cos^{-1}(\hat{n}_1 \cdot \hat{n}_{sc}) \text{ with } \hat{n}_{sc} = \frac{\hat{z} \times \vec{P}_1}{|\hat{z} \times \vec{P}_1|}, \quad (32)$$

$$\cos\theta^* = \frac{\vec{P}_1 \cdot \hat{z}}{|\vec{P}_1|}, \quad (33)$$

$$\cos\theta_1 = -\frac{\vec{P}_2 \cdot \vec{u}_1}{|\vec{P}_2||\vec{u}_1|}. \quad (34)$$

For the first three variables, all the momenta are measured in the rest frame of resonance R , while for the last one, all the momenta are measured in the rest frame of vector boson V_1 . These variables have been used in the context of resonance discrimination in the literature, and they show distinctive structures depending on quantum numbers of each resonance (see, for example, Ref. [46]).

We here study the above-listed observables in the analysis of $R \rightarrow W^+W^-$, and show the distributions in Fig. 6. The distributions are plotted with parton-level events with a 10% of Gaussian smearing onto energy of each final state particle for more realistic Monte Carlo simulation. Again, events were generated by `MadGraph_aMC@NLO` [49] together with the default set of parton distributions `NNPDF23` [50] at the center of mass energy of 13 TeV. Table I summarizes our parameter choices for each scenario. All the parameters *not* listed in the table are simply taken to be zero. Note that this choice of parameters is made only for the purpose of illustration of different kinematic distributions for each scenario. We find that the shape is not strongly dependent on parameters. The mass and the total decay

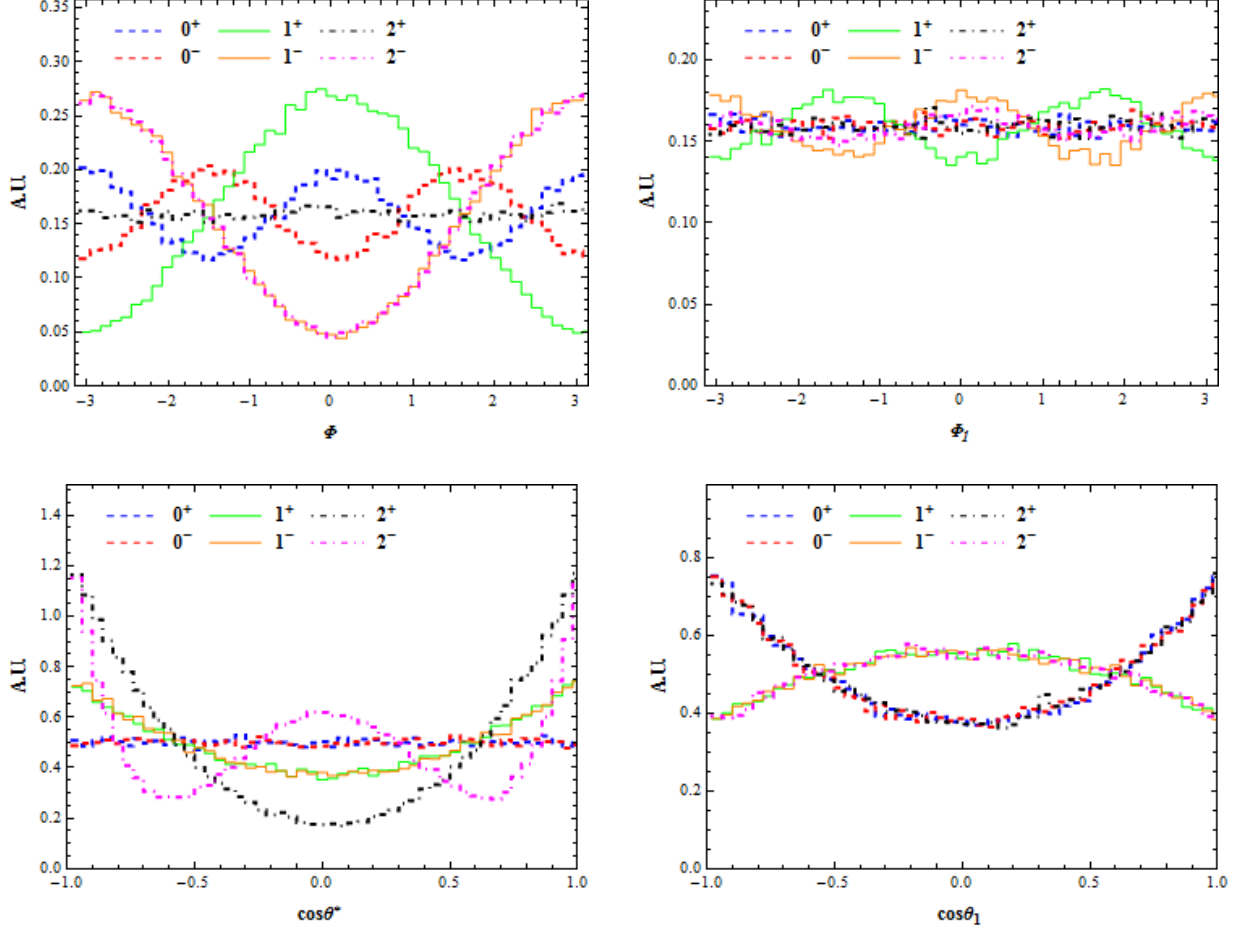


FIG. 6. Unit-normalized distributions in Φ (upper left panel), Φ_1 (upper right panel), $\cos\theta^*$ (lower left panel), and $\cos\theta_1$ (lower right panel) for the resonance decay into two W gauge bosons. The spin and CP state of the resonance of interest is represented by J^{CP} .

width are fixed to be 2 TeV and 0.1 TeV, correspondingly. We remark that the spin-0 and CP-even spin-2 resonances are produced via gluon fusion while the spin-1 and CP-odd spin-2 resonances are produced via quark annihilation. The observables of Φ , Φ_1 , $\cos\theta^*$, and $\cos\theta_1$ are exhibited in the upper left panel, the upper right panel, the lower left panel, and the lower right panel, respectively. Different spin and CP states are symbolized by J^{CP} , and they are histogrammed as follows: CP-even scalar by the blue dashed, CP-odd scalar by the red dashed, CP-even vector by the green solid, CP-odd vector by the orange solid, CP-even tensor by the black dot-dashed, and CP-odd tensor by the magenta dot-dashed. In

particular, the theory prediction for $\cos\theta^*$ distributions is readily derived as follows:

$$\frac{d\sigma}{d\cos\theta^*} \sim \begin{cases} 1, & \text{for } gg \rightarrow 0^+, 0^- \rightarrow W^+W^- \\ 1 + \cos^2\theta^*, & \text{for } q\bar{q} \rightarrow 1^+, 1^- \rightarrow W^+W^- \\ 1 + 6\cos^2\theta^* + \cos^4\theta^*, & \text{for } gg \rightarrow 2^+ \rightarrow W^+W^- \\ 1 - 3\cos^2\theta^* + 4\cos^4\theta^*, & \text{for } q\bar{q} \rightarrow 2^- \rightarrow W^+W^- \end{cases}. \quad (35)$$

which can be directly compared with experimental data.

First of all, we observe that the angular distributions with the Gaussian smearing are very similar to those without any smearing, from which we expect that the angular distributions are insensitive to detector effects such as jet energy resolution. Moving onto Fig. 6, we clearly see that these observables are useful enough to distinguish potential scenarios associated with diboson resonances. For example, the CP-even vector resonance (green solid histograms) shows distinctive behaviors in all four observables. Furthermore, the unique features according to different spin and CP states in those variables can be used for cross-checks. Note that one single distribution can not discriminate different scenarios and it is important to consider all possible kinematic correlations. Finally, we remark that similar analyses can be straightforwardly applicable to other diboson resonances such as $R \rightarrow h\gamma$, $R \rightarrow hZ$ and $R \rightarrow Z\gamma$ so that more information can be extracted to confirm the underlying physics governing the observed phenomena.

VI. SUMMARY

Recently, the ATLAS collaboration has reported some excesses in searches for diboson resonances using jet-substructure techniques. The excesses show up in the invariant mass of W^+W^- , $W^\pm Z$ and ZZ at around 2 TeV. It has been discussed in literature that about 20% of the events in at least one signal region belong to all three categories, which indicates that these “resonances” may be explained by one single particle rather than two.

In this paper, we have explored a possible new physics interpretation of the ATLAS diboson excess without assuming any particular model but in an model-independent manner. We considered the effective operators for scalar, vector, and tensor resonances with different CP properties and have shown that each scenario may explain the ATLAS diboson excess without contradicting other constraints. Symmetries of each scenario predict signals in other final states such as $Z\gamma$ and $\gamma\gamma$ in the cases of scalar and CP-even tensor resonances; $Z\gamma$ and

Zh , γh at a smaller rate in the cases of vector and CP-odd tensor resonances. Especially, the dijet, $t\bar{t}$, $Z\gamma$, Zh , and γh resonance searches at the LHC run II may confirm or constrain these scenarios.

With limited statistics, all these scenarios provide a relatively good fit to the data. However, a further accumulation of data might reveal the real identity of the resonance. We showed a few examples of kinematic distributions, which are sensitive to the CP property and spin of the resonance. We strongly encourage experimental collaborations to look at these kinematic correlations.

APPENDIX

In this appendix, we summarize the useful formulas for the decay rates for scalar and tensor resonances.

A. CP-even scalar

For interaction Lagrangian $\mathcal{L} = -c_{V_1 V_2} \frac{\phi}{\Lambda} F_{V_1}^{\mu\nu} F_{V_2 \mu\nu}$, the decay width of ϕ to $V_1 V_2$ is given as

$$\Gamma(\phi \rightarrow V_1 V_2) = \frac{s_V |c_{V_1 V_2}|^2}{8\pi} \cdot \left(\frac{m_\phi^3}{\Lambda^2} \right) \cdot \mathcal{F}\left(\frac{m_1}{m_\phi}, \frac{m_2}{m_\phi}\right), \quad (36)$$

$$\mathcal{F}(x_1, x_2) = (1 - (x_1 + x_2)^2)^{1/2} (1 - (x_1 - x_2)^2)^{1/2} (1 + x_1^4 + x_2^4 - 2(x_1^2 + x_2^2) + 4x_1^2 x_2^2) \quad (37)$$

where s_V is symmetric factor, which is 1 for $V_1 \neq V_2$ and 2 for $V_1 = V_2$, respectively.

B. CP-odd scalar

For interaction Lagrangian $\mathcal{L} = -c_{V_1 V_2} \frac{A}{\Lambda} F_{V_1}^{\mu\nu} \tilde{F}_{V_2 \mu\nu}$, the decay width of A to $V_1 V_2$ is given as

$$\Gamma(A \rightarrow V_1 V_2) = \frac{s_V |c_{V_1 V_2}|^2}{2\pi} \cdot \left(\frac{m_A^3}{\Lambda^2} \right) \cdot \mathcal{G}\left(\frac{m_1}{m_A}, \frac{m_2}{m_A}\right), \quad (38)$$

$$\mathcal{G}(x_1, x_2) = (1 - (x_1 + x_2)^2)^{3/2} (1 - (x_1 - x_2)^2)^{3/2} \quad (39)$$

where s_V is symmetric factor, which is 1 for $V_1 \neq V_2$ and 2 for $V_1 = V_2$, respectively.

C. CP-even tensor

For spin-2 tensor with mass m_G , the interaction Lagrangian is $\mathcal{L} = -c_{V_1 V_2} \frac{\mathcal{G}_{\mu\nu}}{\Lambda} F_{V_1}{}^\mu{}_\lambda F_{V_2}{}^{\lambda\nu}$ and the decay width of $\mathcal{G}_{\mu\nu} \rightarrow V_1 V_2$ is given as

$$\Gamma(\mathcal{G}_{\mu\nu} \rightarrow V_1 V_2) = \frac{s_V |c_{V_1 V_2}|^2 m_G^3}{160\pi\Lambda^2} \mathcal{H}\left(\frac{m_1}{m_h}, \frac{m_2}{m_h}\right), \quad (40)$$

where the convenient dimensionless function, $\mathcal{H}(x, y)$, for some interesting cases are

$$\mathcal{H}(x, x) = \sqrt{1 - 4x^2}(1 - 3x^2 + 6x^4), \quad (41)$$

$$\mathcal{H}(x, 0) = (1 - x^2)^3(1 + \frac{1}{2}x^2 + \frac{1}{6}x^4) \quad (42)$$

and the symmetric factor s_V is 1 for $V_1 \neq V_2$ and 2 for $V_1 = V_2$, respectively.

ACKNOWLEDGMENTS

We thank the Center for Theoretical Underground Physics and Related Areas (CETUP* 2015) for hospitality and partial support during the completion of this work. Especially we are grateful to Barbara Szczerbinska for all the arrangements and encouragement. We also thank Kingman Cheung, Pyungwon Ko, Jong-Chul Park, Veronica Sanz and Yeo Woong Yoon for helpful discussion. This work is partially supported by the Basic Science Research Program through the National Research Foundation of Korea funded by the Ministry of Education, Science and Technology (2013R1A1A2064120 and 2013R1A1A2007919). D. K. is supported by the LHC Theory Initiative postdoctoral fellowship (NSF Grant No. PHY-0969510), and K. K. is supported by the U.S. DOE under Grant No. DE-FG02-12ER41809.

-
- [1] G. Aad *et al.* [ATLAS Collaboration], arXiv:1506.00962 [hep-ex].
 - [2] L. A. Anchordoqui, I. Antoniadis, H. Goldberg, X. Huang, D. Lust and T. R. Taylor, arXiv:1507.05299 [hep-ph].
 - [3] W. Chao, arXiv:1507.05310 [hep-ph].
 - [4] V. Sanz, arXiv:1507.03553 [hep-ph].
 - [5] H. S. Fukano, S. Matsuzaki and K. Yamawaki, arXiv:1507.03428 [hep-ph].
 - [6] G. Cacciapaglia, A. Deandrea and M. Hashimoto, arXiv:1507.03098 [hep-ph].

- [7] C. W. Chiang, H. Fukuda, K. Harigaya, M. Ibe and T. T. Yanagida, arXiv:1507.02483 [hep-ph].
- [8] B. A. Dobrescu and Z. Liu, arXiv:1507.01923 [hep-ph].
- [9] A. Carmona, A. Delgado, M. Quiros and J. Santiago, arXiv:1507.01914 [hep-ph].
- [10] T. Abe, T. Kitahara and M. M. Nojiri, arXiv:1507.01681 [hep-ph].
- [11] B. C. Allanach, B. Gripaios and D. Sutherland, arXiv:1507.01638 [hep-ph].
- [12] T. Abe, R. Nagai, S. Okawa and M. Tanabashi, arXiv:1507.01185 [hep-ph].
- [13] G. Cacciapaglia and M. T. Frandsen, arXiv:1507.00900 [hep-ph].
- [14] Q. H. Cao, B. Yan and D. M. Zhang, arXiv:1507.00268 [hep-ph].
- [15] J. Brehmer, J. Hewett, J. Kopp, T. Rizzo and J. Tattersall, arXiv:1507.00013 [hep-ph].
- [16] A. Thamm, R. Torre and A. Wulzer, arXiv:1506.08688 [hep-ph].
- [17] Y. Gao, T. Ghosh, K. Sinha and J. H. Yu, arXiv:1506.07511 [hep-ph].
- [18] A. Alves, A. Berlin, S. Profumo and F. S. Queiroz, arXiv:1506.06767 [hep-ph].
- [19] J. A. Aguilar-Saavedra, arXiv:1506.06739 [hep-ph].
- [20] B. A. Dobrescu and Z. Liu, arXiv:1506.06736 [hep-ph].
- [21] K. Cheung, W. Y. Keung, P. Y. Tseng and T. C. Yuan, arXiv:1506.06064 [hep-ph].
- [22] D. B. Franzosi, M. T. Frandsen and F. Sannino, arXiv:1506.04392 [hep-ph].
- [23] J. Hisano, N. Nagata and Y. Omura, arXiv:1506.03931 [hep-ph].
- [24] H. S. Fukano, M. Kurachi, S. Matsuzaki, K. Terashi and K. Yamawaki, arXiv:1506.03751 [hep-ph].
- [25] Y. Omura, K. Tobe and K. Tsumura, arXiv:1507.05028 [hep-ph].
- [26] C. H. Chen and T. Nomura, arXiv:1507.04431 [hep-ph].
- [27] L. A. Anchordoqui, I. Antoniadis, H. Goldberg, X. Huang, D. Lust and T. R. Taylor, arXiv:1507.05299 [hep-ph].
- [28] W. Chao, arXiv:1507.05310 [hep-ph].
- [29] W. D. Goldberger and M. B. Wise, Phys. Rev. Lett. **83**, 4922 (1999) [hep-ph/9907447].
- [30] G. F. Giudice, R. Rattazzi and J. D. Wells, Nucl. Phys. B **595**, 250 (2001) [hep-ph/0002178].
- [31] S. C. Park, H. S. Song and J. H. Song, Phys. Rev. D **65**, 075008 (2002) [hep-ph/0103308].
- [32] S. Bae, P. Ko, H. S. Lee and J. Lee, Phys. Lett. B **487**, 299 (2000) [hep-ph/0002224].
- [33] C. Csaki, M. L. Graesser and G. D. Kribs, Phys. Rev. D **63**, 065002 (2001) [hep-th/0008151].
- [34] S. C. Park and H. S. Song, Phys. Lett. B **506**, 99 (2001) [hep-ph/0103072].

- [35] G. Aad *et al.* [ATLAS Collaboration], arXiv:1504.05511 [hep-ex].
- [36] CMS Collaboration [CMS Collaboration], CMS-PAS-EXO-12-045.
- [37] A. Belyaev, N. D. Christensen and A. Pukhov, *Comput. Phys. Commun.* **184**, 1729 (2013) [arXiv:1207.6082 [hep-ph]].
- [38] J. Alwall, M. Herquet, F. Maltoni, O. Mattelaer and T. Stelzer, *JHEP* **1106**, 128 (2011) [arXiv:1106.0522 [hep-ph]].
- [39] V. Khachatryan *et al.* [CMS Collaboration], *Phys. Rev. D* **91**, no. 5, 052009 (2015) [arXiv:1501.04198 [hep-ex]].
- [40] G. Aad *et al.* [ATLAS Collaboration], *Phys. Rev. D* **91**, no. 5, 052007 (2015) [arXiv:1407.1376 [hep-ex]].
- [41] H. M. Lee, M. Park and W. I. Park, *Phys. Rev. D* **86** (2012) 103502 [arXiv:1205.4675 [hep-ph]].
- [42] H. M. Lee, M. Park and V. Sanz, *JHEP* **1303** (2013) 052 [arXiv:1212.5647 [hep-ph]].
- [43] H. M. Lee, M. Park and V. Sanz, *Eur. Phys. J. C* **74** (2014) 2715 [arXiv:1306.4107 [hep-ph]]; H. M. Lee, M. Park and V. Sanz, *JHEP* **1405** (2014) 063 [arXiv:1401.5301 [hep-ph]].
- [44] E. Dudas, Y. Mambrini, S. Pokorski and A. Romagnoni, *JHEP* **0908** (2009) 014 [arXiv:0904.1745 [hep-ph]].
- [45] R. Fok, C. Guimaraes, R. Lewis and V. Sanz, *JHEP* **1212** (2012) 062 [arXiv:1203.2917 [hep-ph]].
- [46] S. Bolognesi, Y. Gao, A. V. Gritsan, K. Melnikov, M. Schulze, N. V. Tran and A. Whitbeck, *Phys. Rev. D* **86** (2012) 095031 [arXiv:1208.4018 [hep-ph]].
- [47] G. Aad *et al.* [ATLAS Collaboration], *Phys. Lett. B* **738**, 428 (2014) [arXiv:1407.8150 [hep-ex]].
- [48] F. Yu, arXiv:1308.1077 [hep-ph].
- [49] J. Alwall, R. Frederix, S. Frixione, V. Hirschi, F. Maltoni, O. Mattelaer, H.-S. Shao and T. Stelzer *et al.*, *JHEP* **1407**, 079 (2014) [arXiv:1405.0301 [hep-ph]].
- [50] R. D. Ball, V. Bertone, S. Carrazza, C. S. Deans, L. Del Debbio, S. Forte, A. Guffanti and N. P. Hartland *et al.*, “Parton distributions with LHC data,” *Nucl. Phys. B* **867**, 244 (2013) [arXiv:1207.1303 [hep-ph]].